LASER & PHOTONICS REVIEWS

www.lpr-journal.org

REPRINT

WILEY-VCH

Abstract Plasmon resonances and extraordinary light scatterings of a nanoparticle with radial anisotropy are studied and summarized. The coupling between localized surface plasmons and far-field quantities is discussed. It is found that the presence of radial anisotropy redistributes the localization of plasmons and also results in certain novel phenomena in the far zone, which provide the possibility of scattering control such as electromagnetic transparency, enhanced scattering cross section, etc. The nonlinear optical response is explored in order to yield deeper physical insight into the interaction between plasmons and incident light.

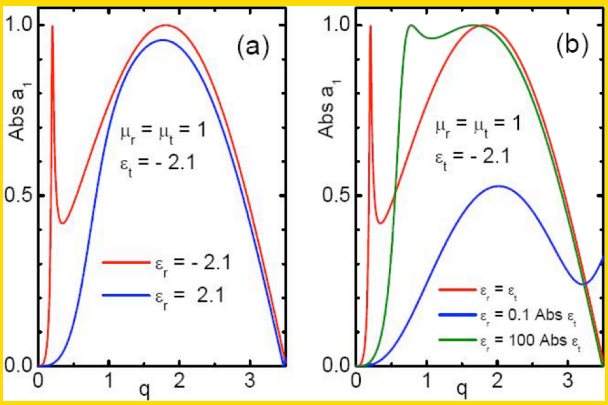

Nondissipative damping in the dipolar mode in a radial anisotropic sphere when the transversal permittivity $\epsilon_t = -2.1$ is near the surface plasmon resonance with positive ϵ_r ($A_e < 0$) at different scales.

© 2010 by WILEY-VCH Verlag GmbH & Co. KGaA, Weinheim

Light scattering from anisotropic particles: propagation, localization, and nonlinearity

Chengwei Qiu[1,2,*], *Lei Gao*[3], *John D. Joannopoulos*[2], *and Marin Soljačić*[2]

[1] Department of Electrical and Computer Engineering, National University of Singapore, Kent Ridge 119260, Republic of Singapore
[2] Department of Physics, Massachusetts Institute of Technology, Cambridge, Massachusetts 02139, USA
[3] Department of Physics, Soochow University, Suzhou, Jiangsu 215006, China

Received: 16 December 2008, Revised: 20 March 2009, Accepted: 25 March 2009
Published online: 23 April 2009

Key words: Localized plasmon, radial anisotropy, nonlinear optical response, transparency, enhanced scattering.

PACS: 42.25.Fx, 42.65.An, 78.67.Bf, 52.40.Db

1. Introduction

Light scattering by arbitrary three-dimensional (3D) objects is a topic of interest in many scientific communities, e.g., astrophysics, atmospheric physics, remote sensing, electromagnetics, and photonics. Scattering from isotropic homogeneous spheres was first formulated by Lorentz [1] and Mie [2], which set the foundations of many following investigations for particular shapes or more complex media. Some peculiarities of light scattering for isotropic materials were found recently for the case of weakly dissipating materials near plasmon resonance frequencies. For these isotropic materials, the classical Rayleigh scattering does not hold and can be replaced by anomalous light scattering [3]. This anomalous light scattering is associated with complex patterns of near and far fields, in contrast to that of Rayleigh scattering. It also demonstrates an extraordinary scattering effect [4], which is similar to quantum scattering by a potential with quasi-discrete levels exhibiting Fano resonances [5]. Another interesting effect refers to active random isotropic media which support optical light enhancement [6].

Light diffraction and scattering by anisotropic particles is a field of particular interest due to vast technological and biological applications. Many solid materials in nature are anisotropic, e.g., polar crystallites made of orientational

* Corresponding author: e-mail: cwq@mit.edu

© 2010 by WILEY-VCH Verlag GmbH & Co. KGaA, Weinheim

molecules are generally both anisotropic and collective. The anisotropy stems from the lack of symmetry in the local atomic environment whilst the collectivity is caused by the dense grouping of molecules. Such anisotropy can be easily established from composite crystals [7], graphitic multishells [8], or spherically stratified media [9], and indeed found in membranes containing mobile charges [10]. Basically, there are two anisotropies, i.e., Cartesian anisotropy and radial anisotropy. Mie theory has been extended to treat Cartesian anisotropic particles in different 3D geometries, such as spheres, ellipsoids, and arbitrary shapes. In the case of arbitrary 3D Cartesian anisotropic particles, numerical solutions are more powerful since extended analytical solutions in this regard can only study spherical cases [11]. However, the anisotropic response of a spherical particle made of crystalline materials [12] has received less attention in spite of its importance for the technologies of embedding of artificial particles and biomedical detection. Recently, scattering of light by Cartesian anisotropic particles has been analyzed in [13, 14], but the material is primarily characterized in rectangular coordinates and treated by a differential theory.

Another special interest presents the spherical particles with radial anisotropies [15–17]. Especially in medical applications and bio-engineering, the light scattering by radial anisotropic particles provides insight into the detail of interaction of embedded/injected bioparticles with the microwave and/or optical illumination by external devices [18–20], which could help to locate some abnormal proteins [21]. It is expected that molecules in spherical particles with radial anisotropy are at least partially oriented with respect to the normal direction to the surface [22–24]. Such orientation of molecules can be easily included into the theory considering the particle as a uniaxial anisotropic medium with the principal optical axis along the local normal direction to the surface. The complex dielectric/magnetic tensorial components ϵ_r (μ_r) and ϵ_t (μ_t) correspond to the parameters normal to and tangential to the local surface (local optical axis [25]), respectively. This problem can be investigated systematically on the basis of the exact solution of Maxwell's equations, which presents the modification of the Mie theory to the diffraction by an anisotropic sphere, including both electric and magnetic anisotropy ratios. Note that the anisotropy and the material parameters involved are described in spherical morphology in which the local $\widehat{x}$, $\widehat{y}$, and $\widehat{z}$ are replaced by $\widehat{r}$, $\widehat{\theta}$, and $\widehat{\phi}$.

Such radially anisotropic materials are receiving great attention recently from both scientific and engineering communities. It has been reported that the classic spherical cloak [26] can be realized by materials with radial anisotropy using a coordinate transformation [27], which were primarily presented in the optics limit or static cases. More recently, high-order transformations for spherical invisible cloaks have been proposed which would improve the invisibility performance and/or alleviate the material parameter restriction [28–30]. However, it is noted that the parameters of radially anisotropic materials used in classic spherical cloaks are position dependent, leading to different eigenmodes from those with position-independent parameters. The light scattering by such radially anisotropic materials can be quite unusual [31], because of the anisotropy, and the nonlinear effects are also controllable via the radial anisotropy [32–34].

Thus, the purpose of this review paper is to provide the targeted audience with a mini-summary of both the Cartesian and the radial anisotropic effects on the scattering patterns, energy localization, and other extraordinary physics phenomena, on the basis of exact and compact solutions for light scattering by spherical particles with uniaxial anisotropy defined in rectangular and spherical coordinates, respectively. Note that we only discuss spherical particles throughout. This review is organized as follows: in Sect. 2, we will quite briefly discuss the anomalous scattering in the presence of no anisotropy, whose coefficients will be compared with the radial anisotropic case; in Sect. 3, a general numerical algorithm is reviewed for the anisotropy in Cartesian coordinates, which can model arbitrary shapes; in Sect. 4, the theoretical characterization of electromagnetic wave interactions with a single radial anisotropic sphere is reviewed and the role of radial anisotropy in anomalous light scattering and surface plasmonics is presented; in Sects. 4 and 5, a core-shell system in which one layer is occupied by a radial anisotropic medium is investigated where the scattering reduction, near-field perturbation, and nonlinear response are discussed; a short conclusion is provided in Sect. 6.

2. Preliminaries

A spherical particle can be used as a lens for focusing laser radiation. It has potential applications in high-density data storage and high-resolution optical lithography for nanodevice fabrication. The problem of electromagnetic scattering by isotropic spherical particles has been well established by Mie theory [35], which indicates that a small transparent particle can lead to a strong field enhancement as a near-field lens. In the near field of the particle, the energy flux would be localized in the area below the diffraction limit, which is employed for applications in optical devices and nanopatterning [36–40].

For an optically large transparent sphere (the radius $a \gg \lambda$), geometrical optics [41] can be used for the ray tracing and one can consequently determine the field intensity distribution in the vicinity of the particle [42]. In order to include the diffraction and aberration, a Bessoid integral can be used to give a more accurate picture of the fields of a big particle [43]. Nevertheless, a detailed calculation can be performed by Mie theory in this case.

When the particle size is sufficiently small compared with the incident wavelength, Rayleigh scattering dominates and the far field is ∞-shaped. However, Rayleigh scattering does not hold in the case of small particles near plasmon resonance frequencies. An easy proof can be found in the expression of the Rayleigh scattering cross section

© 2010 by WILEY-VCH Verlag GmbH & Co. KGaA, Weinheim

(SCS): the denominator contains a term of $\epsilon + 2$, meaning that SCS will diverge if $\mathrm{Re}[\epsilon] = -2$ and $\mathrm{Im}[\epsilon] \to 0$. Under such a circumstance, anomalous scattering replaces Rayleigh scattering, and a two-fold process comes into play: (1) transformation of incident light into localized plasmons, resulting in dissipative damping, and (2) transformation of localized plasmons into scattered light, leading to radiative damping. Owing to the radiative damping, the scattering has finite values even at exact plasmon resonances. However, the Rayleigh scattering approximation is valid only when this radiative damping is negligibly smaller than the dissipative damping. If the radiative damping becomes dominant, anomalous scattering occurs instead of Rayleigh scattering, which results in giant optical resonances, enhanced scattering cross sections, and a complicated energy distribution. For small-sized plasmonic spheres, there are two primary scattering coefficients involved, i.e., a_1 (electric) and b_l (magnetic) within the framework of Mie theory:

$$a_l = \frac{\Re_l^{(a)}}{\Re_l^{(a)} + i\Im_l^{(a)}}, \qquad b_l = \frac{\Re_l^{(b)}}{\Re_l^{(b)} + i\Im_l^{(b)}}, \tag{1}$$

where

$$\Re_l^{(a)} = n\psi_l'(q)\psi_l(nq) - \psi_l(q)\psi_l'(nq), \tag{2}$$

$$\Im_l^{(a)} = n\chi_l'(q)\psi_l(nq) - \chi_l(q)\psi_l'(nq), \tag{3}$$

$$\Re_l^{(b)} = n\psi_l(q)\psi_l'(nq) - \psi_l'(q)\psi_l(nq), \tag{4}$$

$$\Im_l^{(b)} = n\chi_l(q)\psi_l'(nq) - \chi_l'(q)\psi_l(nq). \tag{5}$$

In the formulas above, $n = \sqrt{\epsilon}$ denotes the relative refractive index of the sphere at radius a and $q = k_0 a$ is the so-called size parameter. Here, $\psi_l(x) = \sqrt{\pi x/2} J_{l+1/2}(x)$, $\chi_l(x) = \sqrt{\pi x/2} N_{l+1/2}(x)$, and the prime indicates differentiation with respect to the entire argument. Now, one can easily see that if the particle is not at its resonance, $\Re << \Im$ holds in Eq. (1), so that only the dipole mode ($l = 1$) needs to be considered, which is the basis of Rayleigh approximation. If the particle is at resonant frequency, $\Re >> \Im$ holds in Eq. (1), and then the amplitudes of a_l and b_l will be cut off at 1, resulting in a finite large SCS instead of infinity produced by Rayleigh approximation. The scattering, extinction, and absorption SCS normalized by πa^2 (the cross section of the sphere) are

$$Q_{\mathrm{sca}} = \frac{2}{q^2}\sum_{n=1}^{\infty}(2l+1)\left(|a_l|^2 + |b_l|^2\right), \tag{6}$$

$$Q_{\mathrm{ext}} = \frac{2}{q^2}\sum_{n=1}^{\infty}(2l+1)\Re[a_l + b_l], \tag{7}$$

$$Q_{\mathrm{abs}} = Q_{\mathrm{ext}} - Q_{\mathrm{sca}}. \tag{8}$$

Surprisingly, the resonant peak value of the quadrupolar contribution prevails over that of the dipolar contribution as shown in Fig. 1, which is in contrast to the conclusion of

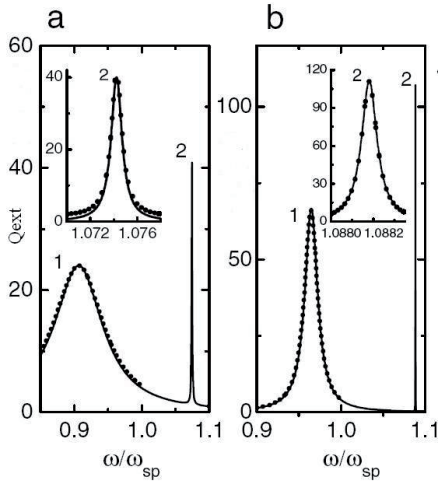

Figure 1 Extinction SCS (Q_{ext}) versus frequency for a metal sphere at the size parameter (a) $q = 0.5$, (b) $q = 0.3$ (reprinted with permission from [45]). The permittivity of a Drude sphere is $\epsilon = 1 - \omega_0^2/\omega^2$, and $\omega_{\mathrm{sp}} = \omega_0/\sqrt{3}$ denotes the dipolar resonant frequency at $q \to 0$. The numbers 1 and 2 correspond to dipole and quadrupole contributions to the extinction SCS, respectively.

Rayleigh scattering. The scattering of arbitrary spherically symmetric resonant objects can also be studied by coupled-mode theory [44].

An even more fascinating effect was found in the vicinity of the quadrupolar resonance, where high sensitivity of the angular distribution of scattered light can be seen for Drude materials with weak dissipation. A very small variation in the incident light frequency changes the scattering diagram from forward scattering to backward scattering, as shown in Fig. 2.

In this case the localized plasmons (polaritons), excited by the incident light in the scattering particle, are equivalent to the quasi-discrete levels in the Fano resonance, while the radiative decay of these excitations plays exactly the same role as tunneling from the quasi-discrete levels in the quantum problem. As a result, the resonance may have a typical N-shaped line with a local maximum, corresponding to constructive interference of different eigenmodes, and a local minimum, corresponding to destructive interference. In particular, the destructive interference may result in considerable, or even complete, suppression of the scattering along any given direction. Thus, the famous Fano resonance [46] was, in fact, hidden in the exact Mie solution.

3. Classification of anisotropy

The presence of anisotropy in the particle will further complicate the extraordinary scattering properties as well as beam steering. In recent years, there has been an increasing interest in characterizing interactions between electromagnetic fields and anisotropic media, owing to their

© 2010 by WILEY-VCH Verlag GmbH & Co. KGaA, Weinheim

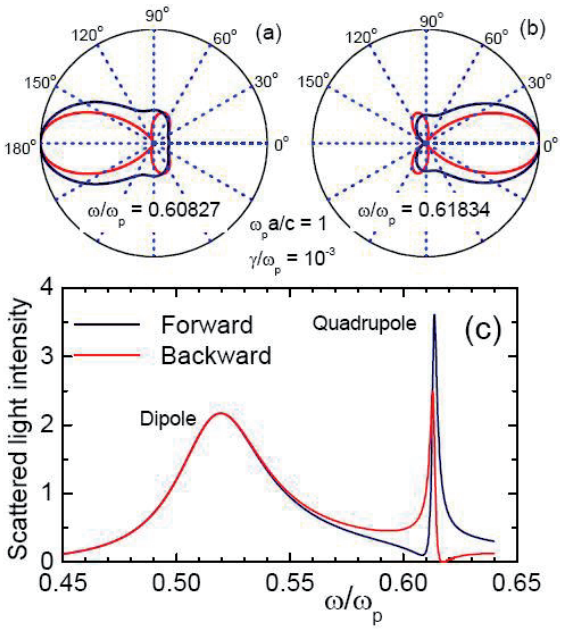

Figure 2 (online color at: www.lpr-journal.org) The angular dependence of light scattering that follows from the exact Mie solution. The dielectric function was described by the Drude model with weak dissipation: $\gamma/\omega_p = 10^{-3}$. The radius is $a = 0.083\lambda$, much smaller than the wavelength. Scattering diagrams in (a) and (b) are defined in the standard way [35] for linearly polarized (red lines) and nonpolarized (blue lines) radiation. In the vicinity of the quadrupole resonance, a fast change of the scattering diagram from forward scattering to backward scattering can be seen within a small variation of frequency. One can see asymmetric forward (blue) and backward (red) scattering profiles associated with the Fano resonance (c).

promising applications in the design and analysis of various novel microwave devices [47–49], subwavelength imaging [50, 51], negative refraction [52–54], and transformation optics [26, 55, 56]. There are two types of anisotropies existing in natural and artificial engineered materials: (1) Cartesian anisotropy (CA); (2) radial anisotropy (RA).

3.1. Cartesian anisotropy of spheres

When the spherical particles possess Cartesian anisotropy, the material parameters are defined as

$$\overline{\boldsymbol{\epsilon}} = \begin{bmatrix} \epsilon_1 & -i\epsilon_2 & 0 \\ i\epsilon_2 & \epsilon_1 & 0 \\ 0 & 0 & \epsilon_3 \end{bmatrix}, \tag{9}$$

$$\overline{\boldsymbol{\mu}} = \begin{bmatrix} \mu_1 & -i\mu_2 & 0 \\ i\mu_2 & \mu_1 & 0 \\ 0 & 0 & \mu_3 \end{bmatrix}, \tag{10}$$

where the unit dyad is $\widehat{\boldsymbol{I}} = \widehat{\boldsymbol{x}}\widehat{\boldsymbol{x}} + \widehat{\boldsymbol{y}}\widehat{\boldsymbol{y}} + \widehat{\boldsymbol{z}}\widehat{\boldsymbol{z}}$. Such a bounded medium with a spherical surface forms a spherical particle of Cartesian anisotropy. To characterize its wave interaction, an analytical method based on multipole expansion [11] has been established by extending Mie theory in isotropic cases to the uniaxial case. Another analytical approach of a dyadic Green's function (DGF) was also investigated even for spherically multilayered structures of anisotropic spheres [57], which is capable of dealing with arbitrary layer number and arbitrary incidences, i.e., plane wave, distributed currents, point source, etc. Those analytical methods are of theoretical and technical importance, whereas they lack robustness in studying arbitrary anisotropic particles in noncanonical shapes or degenerate band edge (DBE) crystals. The unit DBE cells require anisotropic materials as their building blocks [58–60]. Such ensembles can be realized by sapphire and quartz, or by engineered uniaxial layers constructed from textured alternating stacks of two different isotropic dielectrics [61], e.g., Al_2O_3 and $BaTiO_3$. In this connection, numerical algorithms come into play. Specifically, numerical approaches have been proposed based on the method of moments (MoM) [62], the finite-difference time-domain method [63], transmission line modeling [64], the combined field integral equation [65], the coupled dipole approximation method [66], the integral equation [67], and spectral domain Fourier transformation [68].

Given a three-dimensional arbitrarily shaped isotropic object, the scattered electric and magnetic fields can be expressed as

$$\boldsymbol{E} = \boldsymbol{E}^{\rm inc} + \boldsymbol{E}_1^{\rm s} + \boldsymbol{E}_2^{\rm s}, \tag{11}$$

$$\boldsymbol{H} = \boldsymbol{H}^{\rm inc} + \boldsymbol{H}_1^{\rm s} + \boldsymbol{H}_2^{\rm s} \tag{12}$$

or

$$\boldsymbol{E} = \boldsymbol{E}^{\rm inc} - i\omega\boldsymbol{A} - \nabla V - \frac{1}{\epsilon_0}\nabla \times \boldsymbol{F}, \tag{13}$$

$$\boldsymbol{H} = \boldsymbol{H}^{\rm inc} - i\omega\boldsymbol{F} - \nabla U + \frac{1}{\mu_0}\nabla \times \boldsymbol{A}, \tag{14}$$

where $\boldsymbol{E}_1^{\rm s}$ and $\boldsymbol{H}_1^{\rm s}$ are the fields generated by the electric charges and electric currents only; $\boldsymbol{E}_2^{\rm s}$ and $\boldsymbol{H}_2^{\rm s}$ the fields generated by the magnetic charges and magnetic currents only; $\boldsymbol{A}$ ($\boldsymbol{F}$) corresponds to the magnetic (electric) vector potential to be expressed in terms of the electric (magnetic) polarization current $\boldsymbol{J}_{\rm ep}$ ($\boldsymbol{J}_{\rm mp}$); and V (U) corresponds to the electric (magnetic) scalar potential to be expressed in terms of the bounded electric (magnetic) charge density $\rho_{\rm eb}$ ($\rho_{\rm mb}$). If the surface bounded electric (magnetic) charges $\sigma_{\rm eb}$ ($\sigma_{\rm mb}$) are present on the boundary, the contributions due to surface integrals must be added into V and U.

By expressing $\boldsymbol{E}_{1,2}^{\rm s}$ and $\boldsymbol{H}_{1,2}^{\rm s}$ in terms of corresponding polarization currents and bound charge densities, solutions to the total scattered fields can be written using a dyadic

© 2010 by WILEY-VCH Verlag GmbH & Co. KGaA, Weinheim

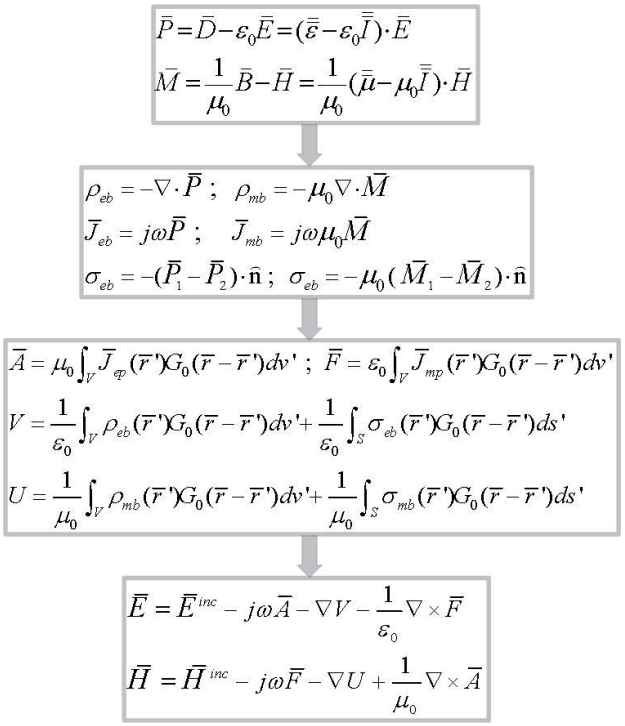

Figure 3 Building blocks and flowchart of solving electromagnetic scattering for arbitrary CA objects.

Green's function in free space ($\widehat{\boldsymbol{G}}_0(\boldsymbol{r},\boldsymbol{r}')$ [69]:

$$\begin{aligned}\boldsymbol{E} &= \boldsymbol{E}^{\mathrm{inc}} - i\omega\mu_0\left[\widehat{\boldsymbol{I}}+\frac{1}{k^2}\nabla\nabla\right]\\ &\quad\cdot\int_V \boldsymbol{J}_{\mathrm{ep}}(\boldsymbol{r}')\,\widehat{\boldsymbol{G}}_0(\boldsymbol{r},\boldsymbol{r}')\,dv'\\ &\quad\nabla\times\int_V \boldsymbol{J}_{\mathrm{mp}}(\boldsymbol{r}')\,\widehat{\boldsymbol{G}}_0(\boldsymbol{r},\boldsymbol{r}')\,dv'\,, \qquad (15)\end{aligned}$$

$$\begin{aligned}\boldsymbol{H} &= \boldsymbol{H}^{\mathrm{inc}} - i\omega\epsilon_0\left[\widehat{\boldsymbol{I}}+\frac{1}{k^2}\nabla\nabla\right]\\ &\quad\cdot\int_V \boldsymbol{J}_{\mathrm{mp}}(\boldsymbol{r}')\,\widehat{\boldsymbol{G}}_0(\boldsymbol{r},\boldsymbol{r}')\,dv'\\ &\quad\nabla\times\int_V \boldsymbol{J}_{\mathrm{ep}}(\boldsymbol{r}')\,\widehat{\boldsymbol{G}}_0(\boldsymbol{r},\boldsymbol{r}')\,dv'\,. \qquad (16)\end{aligned}$$

Note that the relationships between ($\boldsymbol{E}^{\mathrm{inc}}$, $\boldsymbol{H}^{\mathrm{inc}}$) and ($\boldsymbol{P}$, $\boldsymbol{M}$) can be established from the top and bottom blocks in Fig. 3. Consequently, it means that ($\boldsymbol{E}^{\mathrm{inc}}$, $\boldsymbol{H}^{\mathrm{inc}}$) can be further expressed in terms of ($\boldsymbol{J}_{\mathrm{ep}}$, $\boldsymbol{J}_{\mathrm{mp}}$) via the second block in Fig. 3. Eventually, it appears that the unknowns are polarization currents $\boldsymbol{J}_{\mathrm{ep}}$ and $\boldsymbol{J}_{\mathrm{mp}}$, which can be represented by Galerkin's method with RWG basis functions [70, 71].

It should be noted that MoM is usually implemented together with other integral methods, e.g., MoM-VIE (volume integral equation) [72], MoM-CG-FFT [73, 74], MoM-FMM (fast multipole method) [75], and MoM-VSIE (volume-surface integral equation) [76]. That is because the electric and magnetic integral equations (13) and (14) cannot be solved analytically for anisotropic scatterers in noncanonical shape via the vector potential formulation. The MoM technique can be applied to obtain a numerical solution of the integral equations. First, the inhomogeneous scattering problem will be modeled by dividing the medium into many small cells. If the cell is small enough, the material within the cell can be assumed to be homogeneous. Constitutive properties at the centroid of a cell are assigned to the entire cell. Adjacent cells may possess different constitutive properties to model the inhomogeneity. As electromagnetic waves propagate through cells, bound charges and polarization currents may exist inside the cells, and bound surface charges may exist on the cell boundaries. Within the cell, RWG basis functions will be introduced so that the unknown quantities in the integral equations are expanded in terms of these basis functions. Galerkin's testing procedures are used to transform the original integral equations to a MoM matrix equation. The MoM matrix equation can easily be solved to recover the original unknown quantities. A numerical solution of the original integral equations is then established.

To explicitly demonstrate the role of anisotropy in the far-field scattering, we consider an example of a perfectly conducting (PEC) sphere coated by a uniaxial CA shell whose material parameters take the form of

$$\bar{\boldsymbol{\epsilon}} = \epsilon_t(\hat{\boldsymbol{x}}\hat{\boldsymbol{x}}+\hat{\boldsymbol{y}}\hat{\boldsymbol{y}})+\epsilon_z\hat{\boldsymbol{z}}\hat{\boldsymbol{z}}\,, \qquad (17)$$

$$\bar{\boldsymbol{\mu}} = \mu_t(\hat{\boldsymbol{x}}\hat{\boldsymbol{x}}+\hat{\boldsymbol{y}}\hat{\boldsymbol{y}})+\mu_z\hat{\boldsymbol{z}}\hat{\boldsymbol{z}}\,, \qquad (18)$$

which correspond to the reduced case of $\epsilon_2(\mu_2) = 0$, $\epsilon_1(\mu_1) = \epsilon_t(\mu_t)$, and $\epsilon_3(\mu_3) = \epsilon_z(\mu_z)$ in Eqs. (9) and (10).

From Fig. 4, it can be seen that the effect of the electric anisotropy ratio $A_{\mathrm{e}} = \epsilon_t/\epsilon_z$ upon SCS is quite pronounced in the far-field diagrams compared with the curve corresponding to the case of $A_{\mathrm{e}} = 1$ (red lines). It is of particular interest to present the significance of the case when $A_{\mathrm{e}} < 1$. On the E-plane, less-than-unity A_{e} (blue curve) will result in a dramatic decrease of far-field SCS at $\theta \approx 55^\circ$ (the drop is larger than 30 dB compared with either of the other two cases). In contrast, on the H-plane, less-than-unity A_{e} enhances SCS significantly in the vicinity of θ at 108° (the increase is larger than 30 dB with respect to either of the other two cases).

3.2. Radial anisotropy of spheres

In addition to the Cartesian anisotropy (CA), there is another important type of anisotropy, i.e., radial anisotropy (RA). The material tensors in general are given as

$$\bar{\boldsymbol{\epsilon}} = \epsilon_0\begin{bmatrix}\epsilon_r & 0 & 0\\ 0 & \epsilon_t & 0\\ 0 & 0 & \epsilon_t\end{bmatrix}\,, \qquad (19)$$

© 2010 by WILEY-VCH Verlag GmbH & Co. KGaA, Weinheim

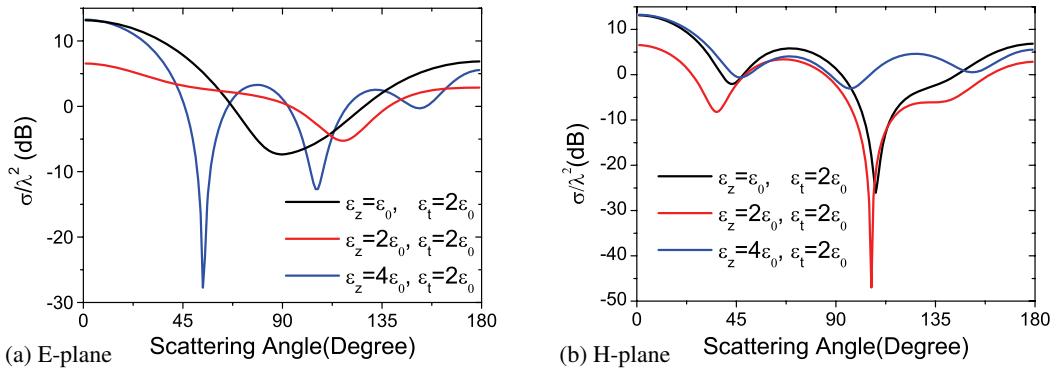

Figure 4 (online color at: www.lpr-journal.org) The effect of anisotropy ratio in bistatic scattering cross sections of a uniaxial-coated PEC sphere: (a) E-plane SCS and (b) H-plane SCS. The radius of the PEC core (a_c) and the thickness (d) of the lossless uniaxial shell are chosen to be $a_c = 0.2\lambda$ and $d = 0.25\lambda$, respectively. The material parameters of the anisotropic coating are assumed to be $\mu_t = 4\mu_0$ and $\mu_z = 2\mu_0$. Three electric anisotropy ratios are considered in particular where the transversal permittivity is fixed at $\epsilon_t = 2\epsilon_0$: (1) $A_e = 2$ (black); (2) $A_e = 1$ (red); (3) $A_e = 0.5$ (blue).

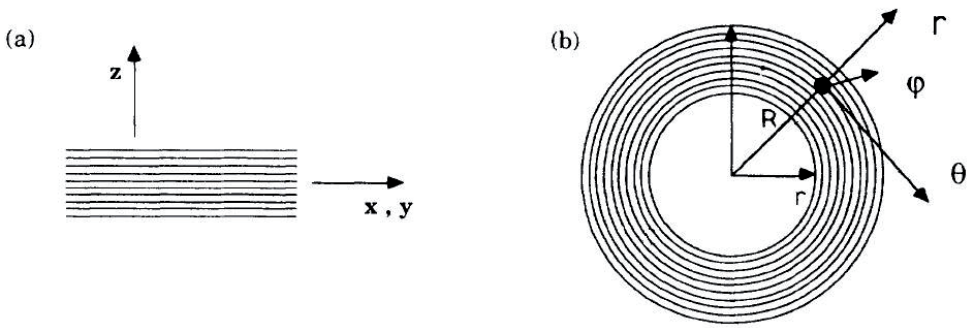

Figure 5 The transformation model between CA and RA for graphite. The dielectric tensor of graphite in (a), which is depicted by Eq. (17), is transposed to the spherical geometry (b).

$$\overline{\boldsymbol{\mu}} = \mu_0 \begin{bmatrix} \mu_r & 0 & 0 \\ 0 & \mu_t & 0 \\ 0 & 0 & \mu_t \end{bmatrix}, \tag{20}$$

where the unit dyad is $\overline{\boldsymbol{I}} = \hat{\boldsymbol{r}}\hat{\boldsymbol{r}} + \hat{\boldsymbol{\theta}}\hat{\boldsymbol{\theta}} + \hat{\boldsymbol{\phi}}\hat{\boldsymbol{\phi}}$.

The transformation from CA to RA is illustrated in Fig. 5, provided that the dielectric continuum is preserved. Obviously, this procedure becomes more rigorous when the inner radius r is much larger than the thickness of graphite $R - r$. Otherwise, angular nonlocality and radial inhomogeneity may arise (which are beyond the scope of the current review), though the major nonlocality arising from the curvature/bending has already been included in Eqs. (19) and (20). Alternatively, such RA can be straightforwardly pictured either by a bundle of conducting strings diverging from a point uniformly in all directions or by a spherically stratified medium with two alternating isotropic layers of different permittivities and permeabilities. If the parameters of those two isotropic materials are assumed to be $(\epsilon_1,\ \mu_1)$ and $(\epsilon_2,\ \mu_2)$, the 'effective' components in Eqs. (19) and (20) can be modeled as

$$\sigma_r = \frac{2}{\sigma_1^{-1} + \sigma_2^{-1}}, \quad \sigma_t = \frac{\sigma_1 + \sigma_2}{2} (\sigma = \epsilon \quad \text{or} \quad \mu), \tag{21}$$

provided that each layer is sufficiently thin.

The research interest in this area of RA was recently initiated by chemists and biologists, and many pioneering works have contributed to the investigations of the heat transfer/absorption in graphite [77], electroencephalography (EEG) [78, 79], biological cell membranes [10], and cloaking [26]. It is now important and necessary to characterize how RA particles interact with waves so as to provide more physical insight into the phenomena such as invisibility, enhanced surface plasmon resonance, and extraordinary scattering.

There is a limited literature regarding the electromagnetic characterization of the scattering properties of RA particles or coated RA particles. This is due to the fact that their local optical axes are along the radial direction normal to the spherical surface, meaning that it is difficult to study these systems by Mie theory or existing numerical methods for CA particles. Here, we will discuss the approach based on modified spherical vector wave functions (MVWFs) and/or Debye potentials for the scattering problems of RA particles. Different eigenmodes in inhomogeneous and homogeneous RA particles are analyzed, and their far-field patterns near surface plasmon resonances are examined.

Let us first study the electromagnetic formulation of a single RA sphere. A more general case was considered in [80] and, if the off-diagonal parameters are zero, E_r

© 2010 by WILEY-VCH Verlag GmbH & Co. KGaA, Weinheim

and H_r are not coupled, as Eq. (3) in [80] shows where the notation is a bit different. It thus implies that TE/TM decomposition can be applied to the study of such uniaxial RA materials characterized by Eqs. (19) and (20). In what follows, we express $\boldsymbol{B}$ and $\boldsymbol{D}$ in terms of the following two sets of scalar Debye potentials:

$$\boldsymbol{B}_{\rm TM} = \nabla \times (\hat{\boldsymbol{r}}\psi_{\rm TM}) \,, \tag{22}$$

$$\boldsymbol{D}_{\rm TE} = -\nabla \times (\hat{\boldsymbol{r}}\psi_{\rm TE}) \,, \tag{23}$$

$$\boldsymbol{B}_{\rm TE} = \frac{1}{i\omega}\left[\nabla \times \left(\overline{\boldsymbol{\epsilon}}^{-1} \cdot \nabla \times (\hat{\boldsymbol{r}}\psi_{\rm TE})\right)\right] \,, \tag{24}$$

$$\boldsymbol{D}_{\rm TM} = \frac{1}{i\omega}\left[\nabla \times \left(\overline{\boldsymbol{\mu}}^{-1} \cdot \nabla \times (\hat{\boldsymbol{r}}\psi_{\rm TM})\right)\right] \,, \tag{25}$$

where $\psi_{\rm TE}$ and $\psi_{\rm TM}$ denote potentials for TE and TM modes with respect to $\hat{\boldsymbol{r}}$ in the spherical coordinate system:

$$\frac{\epsilon_r}{\epsilon_t}\frac{\partial^2\psi_{\rm TM}}{\partial r^2} + \frac{1}{r^2\sin\theta}\frac{\partial}{\partial\theta}\left(\sin\theta\frac{\partial\psi_{\rm TM}}{\partial\theta}\right)\frac{1}{r^2\sin^2\theta}\frac{\partial^2\psi_{\rm TM}}{\partial\phi^2} + \omega^2\mu_0\epsilon_0\mu_t\epsilon_r\psi_{\rm TM} = 0 \,, \tag{26}$$

$$\frac{\mu_r}{\mu_t}\frac{\partial^2\psi_{\rm TE}}{\partial r^2} + \frac{1}{r^2\sin\theta}\frac{\partial}{\partial\theta}\left(\sin\theta\frac{\partial\psi_{\rm TE}}{\partial\theta}\right)\frac{1}{r^2\sin^2\theta}\frac{\partial^2\psi_{\rm TE}}{\partial\phi^2} + \omega^2\mu_0\epsilon_0\mu_r\epsilon_t\psi_{\rm TE} = 0 \,. \tag{27}$$

We apply the variable separation

$$\psi = R(r)\Theta(\theta)\Phi(\phi) \tag{28}$$

to those partial differential equations above, and we have the resultant equations

$$\frac{\epsilon_r}{\epsilon_t}\frac{d^2}{dr^2} + \left(k_0^2\epsilon_r\mu_t - \frac{\alpha}{r^2}\right)R = 0 \,, \tag{29}$$

$$\frac{1}{\sin\theta}\frac{d}{d\theta}\left(\sin\theta\frac{d\Theta}{d\theta}\right) + \left(\alpha - \frac{\beta}{\sin^2\theta}\right) = 0 \,, \tag{30}$$

$$\frac{d^2\Phi}{d\phi^2} + \beta\Phi = 0 \,, \tag{31}$$

where α and β are integration variables. Following Eq. (31), one has $\beta = m^2$ (m = integer) and $\Phi = e^{jm\phi}$. Eq. (30) is an equation for spherical harmonics, where we should put $\alpha = l(l+1)$ ($l \geq |m|$). By introducing a new variable $\xi = \cos\theta$, Eq. (30) transforms to

$$\frac{d}{d\xi}\left[(1-\xi^2)\frac{d\Theta}{d\xi}\right] + \left[l(l+1) - \frac{m^2}{1-\xi^2}\right]\Theta = 0 \,, \tag{32}$$

which leads to the associated Legendre function $\Theta = P_l^m(\cos\theta)$. The major task is in solving the radial component in Eq. (29). We need to rewrite it as

$$\left\{\frac{d^2}{dr^2} + \left(k_0^2\epsilon_t\mu_t - \frac{\epsilon_t}{\epsilon_r}\frac{l(l+1)}{r^2}\right)\right\}R = 0 \,, \tag{33}$$

which is seemingly unsolvable in a conventional way. However, if we group ϵ_t/ϵ_r and $l(l+1)$ into one term, then it can be rewritten as $v_1(v_1+1) = l(l+1)\epsilon_t/\epsilon_r$, leading to

$$\left\{\frac{d^2}{dr^2} + \left(k_0^2\epsilon_t\mu_t - \frac{v_1(v_1+1)}{r^2}\right)\right\}R = 0 \,. \tag{34}$$

Eq. (34), in fact, falls into the definition of spherical Bessel functions except that the order is no longer an integer. Finally, one has $R(r) = j_{v_1}(k_t r) = \sqrt{\frac{\pi k_t r}{2}}J_{v_1+1/2}(k_t r)$ for Eq. (26), in which $k_t = k_0\sqrt{\epsilon_t\mu_t}$ and $v_1 = [l(l+1)A_{\rm e} + 1/4]^{1/2} - 1/2$. Similarly, one can obtain the radial component $R(r) = j_{v_2}(k_t r) = \sqrt{\frac{\pi k_t r}{2}}J_{v_2+1/2}(k_t r)$ for Eq. (27), in which $v_2 = [l(l+1)A_{\rm m} + 1/4]^{1/2} - 1/2$. $A_{\rm e} = \epsilon_t/\epsilon_r$ and $A_{\rm m} = \mu_t/\mu_r$ correspond to electric and magnetic anisotropic ratios, respectively.

Subsequently, the electromagnetic fields can be expanded as

$$E_r = \frac{\omega}{ik_t^2}\left(\frac{\partial^2}{\partial r^2} + k_t^2\right)\psi_{\rm TM} \,, \tag{35}$$

$$E_\theta = \frac{-1}{\epsilon_0\epsilon_t r\sin\theta}\frac{\partial\psi_{\rm TE}}{\partial\phi} + \frac{\omega}{ik_t^2 r}\frac{\partial^2\psi_{\rm TM}}{\partial r\partial\theta} \,, \tag{36}$$

$$E_\phi = \frac{1}{\epsilon_0\epsilon_t r}\frac{\partial\psi_{\rm TE}}{\partial\theta} + \frac{\omega}{ik_t^2 r\sin\theta}\frac{\partial^2\psi_{\rm TM}}{\partial r\partial\phi} \,, \tag{37}$$

$$H_r = \frac{\omega}{ik_t^2}\left(\frac{\partial^2}{\partial r^2} + k_t^2\right)\psi_{\rm TE} \,, \tag{38}$$

$$H_\theta = \frac{\omega}{ik_t^2 r}\frac{\partial^2\psi_{\rm TE}}{\partial r\partial\theta} + \frac{1}{\mu_0\mu_t r\sin\theta}\frac{\partial\psi_{\rm TM}}{\partial\phi} \,, \tag{39}$$

$$H_\phi = \frac{\omega}{ik_t^2 r\sin\theta}\frac{\partial^2\psi_{\rm TE}}{\partial r\partial\phi} - \frac{1}{\mu_0\mu_t r}\frac{\partial\psi_{\rm TM}}{\partial\theta} \,. \tag{40}$$

Note that the potentials above carry SI units [81]. If one utilizes the potentials in Gaussian units [35], there will be a normalization factor ik_t^2/ω to be multiplied with Eqs. (35)–(40).

The following formulation is very standard, which is analogous to the derivation in isotropic cases, i.e., applying boundary conditions and solving for scattering coefficients. Eventually, we obtain all four scattering coefficients (the first two for scattered waves and the last two for transmitted waves):

$$a_l = \frac{\sqrt{\mu_t/\epsilon_t}j_l(k_0a)j'_{v_1}(k_ta) - j'_l(k_0a)j_{v_1}(k_ta)}{h_n^{(2)'}(k_0a)j_{v_1}(k_ta) - \sqrt{\mu_t/\epsilon_t}h_l^{(2)}(k_0a)j'_{v_1}(k_ta)}T_l \,, \tag{41}$$

$$b_l = \frac{\sqrt{\mu_t/\epsilon_t}j'_l(k_0a)j_{v_2}(k_ta) - j_l(k_0a)j'_{v_2}(k_ta)}{h_n^{(2)}(k_0a)j'_{v_2}(k_ta) - \sqrt{\mu_t/\epsilon_t}h_l^{(2)'}(k_0a)j_{v_2}(k_ta)}T_l \,, \tag{42}$$

© 2010 by WILEY-VCH Verlag GmbH & Co. KGaA, Weinheim

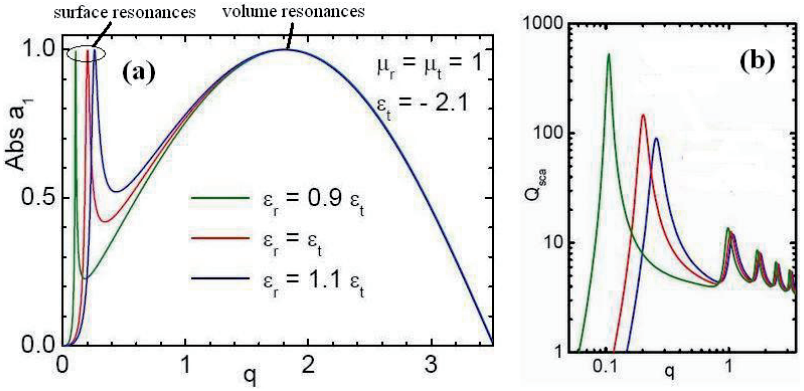

Figure 6 (online color at: www.lpr-journal.org) Surface plasmon resonance for dipole mode (a) and far-field scattering cross section $Q_{\rm sca}$ (b) at various anisotropy ratios with negative ϵ_t and negative ϵ_r ($A_{\rm e} > 0$) (reprinted with permission from [31]).

$$c_l = \frac{i}{\sqrt{\mu_t/\epsilon_t}h_l^{(2)}(k_0a)j'_{v_1}(k_ta) - h_l^{(2)'}(k_0a)j_{v_1}(k_ta)}T_l\,, \tag{43}$$

$$d_l = \frac{i\sqrt{\mu_t\epsilon_t}}{h_l^{(2)}(k_0a)j'_{v_2}(k_ta) - \sqrt{\mu_t/\epsilon_t}h_l^{(2)'}(k_0a)j_{v_2}(k_ta)}T_l\,, \tag{44}$$

$$T_l = \frac{i^{-l}(2l+1)}{l(l+1)}\,. \tag{45}$$

Note that there is a typo in the numerator of Eq. (40) in [81]. For far-field patterns of RA spheres, a_n and b_n are needed, which can be rewritten in an analogy with Eqs. (1)–(5) in isotropic cases

$$A_l = \frac{\Re_l^{(A)}}{\Re_l^{(A)} + i\Im_l^{(A)}}\,, \quad B_l = \frac{\Re_l^{(B)}}{\Re_l^{(B)} + i\Im_l^{(B)}}\,, \tag{46}$$

where

$$\Re_l^{(A)} = n_t\psi'_l(q)\psi_{v_1}(n_tq) - \mu_t\psi_l(q)\psi'_{v_1}(n_tq)\,, \tag{47}$$

$$\Im_l^{(A)} = n_t\chi'_l(q)\psi_{v_1}(n_tq) - \mu_t\chi_l(q)\psi'_{v_1}(n_tq)\,, \tag{48}$$

$$\Re_l^{(B)} = n_t\psi_l(q)\psi'_{v_2}(n_tq) - \mu_t\psi'_l(q)\psi_{v_2}(n_tq)\,, \tag{49}$$

$$\Im_l^{(B)} = n_t\chi_l(q)\psi'_{v_2}(n_tq) - \mu_t\chi'_l(q)\psi_{v_2}(n_tq)\,. \tag{50}$$

Here, $\chi_l(x) = \sqrt{\pi x/2}N_{l+1/2}(x)$ is the Neumann function, $q = k_0a$ presents the so-called Mie size parameter, a is the radius of the RA sphere, and all the primes indicate differentiation with respect to the entire argument. It can be seen that Eqs. (47)–(50) for RA cases are similar to Eqs. (2)–(5) for isotropic cases.

Now, we would like to study the effect of anisotropy upon the scattering by an RA sphere near the surface plasmon resonance. Here, we just assume that the RA sphere has only an electric anisotropy ratio, meaning that $A_{\rm m} = 1$. There are two categories to be investigated: (1) $A_{\rm e} > 0$; (2) $A_{\rm e} < 0$. In both cases, the transverse permittivity ($\epsilon_t = -2.1$) is near the surface plasmon resonance.

In Fig. 6a, the variation of the surface plasmon resonance against the size parameter is well pronounced

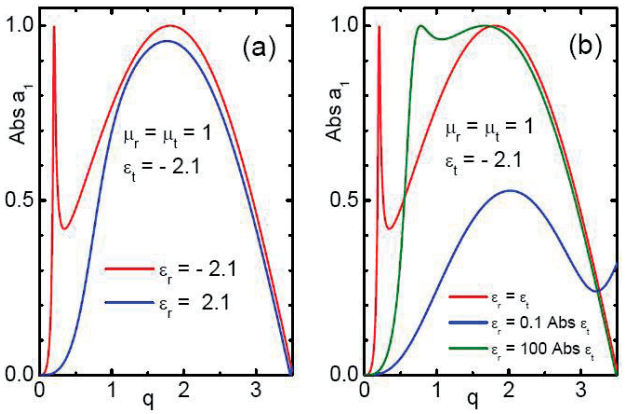

Figure 7 (online color at: www.lpr-journal.org) Scattering amplitude A_1 in Eq. (46) for dipolar resonance in an RA sphere near the surface plasmon resonance with negative ϵ_t and positive ϵ_r ($A_{\rm e} < 0$).

at different anisotropy ratios when size parameters are small enough, and the far-field patterns are influenced consequently as shown in Fig. 6b. However, the positive anisotropy ratio near the surface plasmon resonance has no impact on the volume resonance when q is large.

The situation of an RA sphere near the surface plasmon resonance at $A_{\rm e} < 0$ actually requires that $\epsilon_r > 0$, which presents extraordinary scattering phenomena. In Fig. 7a, we first compare two particular cases corresponding to $A_{\rm e} > 0$ and $A_{\rm e} < 0$, near the surface plasmon resonance. In the first case ($A_{\rm e} = 1$) we can see the usual surface plasmon resonance, while in the second case ($A_{\rm e} = -1$) we can see that the plasmon resonance disappears and a small shift of the resonant value of the first volume resonant mode appears. What is more important, it can be observed that the maximum amplitude of this first volume resonance is not equal to one. In Fig. 7b, we focus on the second case under different scales of the negative $A_{\rm e}$. When $A_{\rm e} \to -\infty$ (blue line in Fig. 7b), one can see a more pronounced effect in the amplitude damping, which is reflected in the nonzero absorption cross section $Q_{\rm abs}$ in Fig. 8a. When $A_{\rm e} \to 0^-$ (green line in Fig. 7b), even the *lost* plasmon resonance

© 2010 by WILEY-VCH Verlag GmbH & Co. KGaA, Weinheim

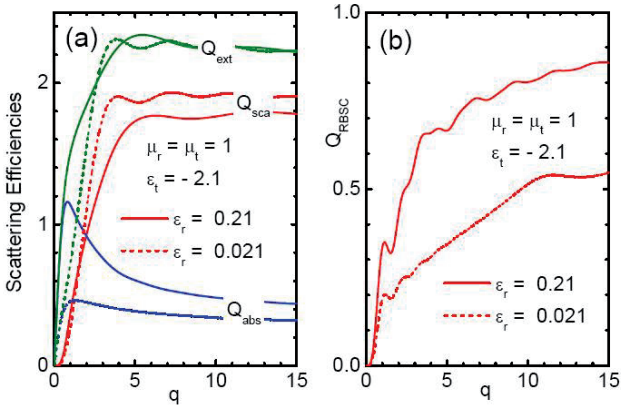

Figure 8 (online color at: www.lpr-journal.org) Scattering efficiencies of an RA sphere of the same type as Fig. 7b but with small positive ϵ_r ($A_e \to -\infty$).

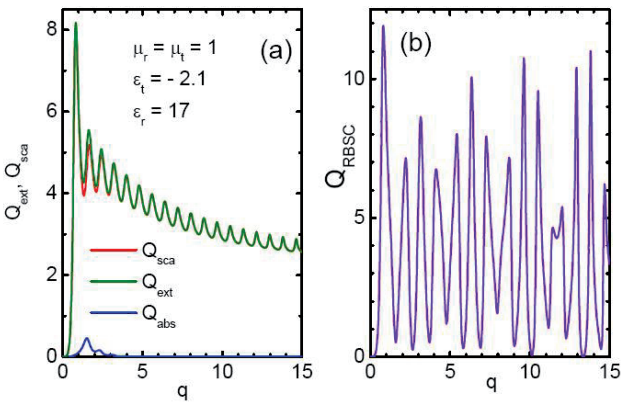

Figure 9 (online color at: www.lpr-journal.org) Scattering efficiencies of an RA sphere of the same type as Fig. 7b but with large positive ϵ_r ($A_e \to 0^-$).

returns, as one can see in Fig. 7b. Thus, it is natural to see that in the case of $A_e \to 0^-$ the nondissipative absorption (see Fig. 9a) will become less and less pronounced since the amplitude damping is being recovered.

Formally, such nondissipative absorptions in Fig. 8a and Fig. 9a, which have no imaginary parts in permittivities, look similar to the effect in dissipative homogeneous media, which has an imaginary part in ϵ. From the physics of plasma we know the situation of Landau damping [82], where the wave dissipates in a collisionless plasma. The physical reason for Landau damping is related to the shift of resonant frequencies of electrons moving at different velocities. Averaging the dielectric permittivity of plasma, where the particle velocities have a Maxwellian distribution function, one formally obtains the nonzero imaginary part of ϵ. The situation of an RA particle at the surface plasmon resonance is quite similar. Here, energy at resonant frequencies of plasmonic oscillations and volume oscillations is redistributed due to the interaction with the radial field oscillations. The total effect formally looks like the absorption within the nondissipative particle. The formal mathematical reason for this effect is related to the behavior of the arbitrary-order spherical Bessel function obtained from Eq. (34). With $A_e < 0$, the order of this function becomes negative. As a result, this function consists of both real and imaginary parts, which produces the mentioned unusual absorption effect.

The radar backscattering is also examined to characterize the role of the anisotropy ratio. It is found that in the category of $A_e < 0$, the backscattering is highly oscillatory at $A_e \to 0^-$ when q increases.

However, if the material parameters in Eqs. (19) and (20) are position independent as a classical spherical cloak ($a \le r \le b$) suggests, i.e., $\epsilon_r = \mu_r = \left(\frac{b}{b-a}\right)\left(\frac{r-a}{r}\right)^2$ and $\epsilon_t = \mu_t = \frac{b}{b-a}$ [26], the eigenmodes will be different from those in Eq. (34) since Eq. (33) becomes

$$\left\{\frac{d^2}{dr^2} + \left(k_0^2 \epsilon_t \mu_t - \frac{n(n+1)}{(r-a)^2}\right)\right\} R = 0\,. \qquad (51)$$

Therefore, we have $R(r) = j_n(k_t(r-a))$, whose order of the spherical Bessel function is an integer again. The field representations can be formulated in a similar way as in [81] in terms of TE and TM potentials except that the difference is now in the argument of the spherical Bessel function instead of its order.

4. Towards light control in coated RA particles

Light control in three-dimensional (3D) photonic crystals is very attractive because they can potentially provide a complete photonic band gap, which can be used to design light-guiding devices. The complete gap in isotropic photonic crystals exists in a diamond structure and inverse-opal face-centered-cubic structure [83, 84]. Therefore, the investigation of anisotropic or even gyrotropic materials seems promising [85]. As is mentioned, RA opens up a way of bending the light and further hiding the coated object [86]. However, such RA needs position-dependent parameters both in permittivity and permeability tensors, resulting in the great difficulty of realizing such particular parameters. Instead, we will revisit the invisibility of a homogeneous RA shell, whose parameters are constant and independent of the radius [87]. The formulation of a coated sphere with RA follows the standard procedures in a single RA sphere described in Sect. 3.2. The field representations in every region can be determined by applying boundary conditions at each interface. The mechanism of achieving transparency relies on the effective-medium theory, which is obviously different from the coordinate transform. By properly tuning the core-shell ratio, the coated sphere with RA can be regarded as a uniform sphere with the effective permittivity and permeability equal to those of free space, leading to

© 2010 by WILEY-VCH Verlag GmbH & Co. KGaA, Weinheim

the invisibility. However, it has its own limitation, i.e., the long-wavelength limit (the size far below the wavelength).

Here, we consider a general case where both the core (designated by subscript c) and the shell (designated by subscript s) are RA materials. The parameters ϵ_{ir}, ϵ_{it}, μ_{ir}, and μ_{it} are relative, $v_{i1}^l = \sqrt{l(l+1)\epsilon_{it}/\epsilon_{ir} + 1/4} - 1/2$, and $v_{i2}^l = \sqrt{l(l+1)\mu_{it}/\mu_{ir} + 1/4} - 1/2$, where $i = \mathrm{c}$ or s. The inner and outer radii are r_0 and R, respectively. Once scattering coefficients for the outermost region have been solved and approximated by asymptotic forms of Bessel and Neumann functions at small arguments, the effective parameters (ϵ_{eff} and μ_{eff}) for such a coated RA sphere can be obtained in an analogy of [88] for isotropic cases, and finally we arrive at a set of equations of the transparency condition for the core-shell ratio

$$\frac{r_0}{R} = \left\{ \frac{(\epsilon_{\mathrm{sr}} v_{\mathrm{s}1}^1 - 1)\left[\epsilon_{\mathrm{cr}} v_{\mathrm{c}1}^1 + \epsilon_{\mathrm{sr}}(v_{\mathrm{s}1}^1 + 1)\right]}{(\epsilon_{\mathrm{sr}} v_{\mathrm{s}1}^1 - \epsilon_{\mathrm{cr}} v_{\mathrm{c}1}^1)\left[1 + \epsilon_{\mathrm{sr}}(1 + v_{\mathrm{s}1}^1)\right]} \right\}^{\frac{1}{(2v_{\mathrm{s}1}^1+1)}}, \tag{52}$$

for nonmagnetic particles, and

$$\frac{r_0}{R} = \left\{ \frac{(\mu_{\mathrm{sr}} v_{\mathrm{s}2}^1 - 1)\left[\mu_{\mathrm{cr}} v_{\mathrm{c}2}^1 + \mu_{\mathrm{sr}}(v_{\mathrm{s}2}^1 + 1)\right]}{(\mu_{\mathrm{sr}} v_{\mathrm{s}2}^1 - \mu_{\mathrm{cr}} v_{\mathrm{c}2}^1)\left[1 + \mu_{\mathrm{sr}}(1 + v_{\mathrm{s}2}^1)\right]} \right\}^{\frac{1}{(2v_{\mathrm{s}2}^1+1)}}, \tag{53}$$

for magnetic materials. Note that the obtained r_0/R by given sets of material parameters has a physical limitation, i.e., $0 < r_0/R < 1$, according to the problem settings. Otherwise, it implies that the present parameters for the core and shell RA materials will never achieve transparency no matter how one changes the filling fraction. Compared with the isotropic coated sphere, the anisotropic coated sphere has introduced more physical parameters for us to achieve transparency. For large particles, quadrupole, octopole, and even higher-order scattering coefficients can still approach zero if the anisotropic ratio and core-shell ratio are tuned accordingly.

In Fig. 10, it can be observed that, once the required condition of the core-shell ratio for transparency is satisfied, the field outside the coated sphere is identical to the incident wave, meaning that the object is invisible to the illumination. However, within the coated RA sphere, the local field E_{loc} is greatly perturbed, which may be used for enhancement of nonlinear effects.

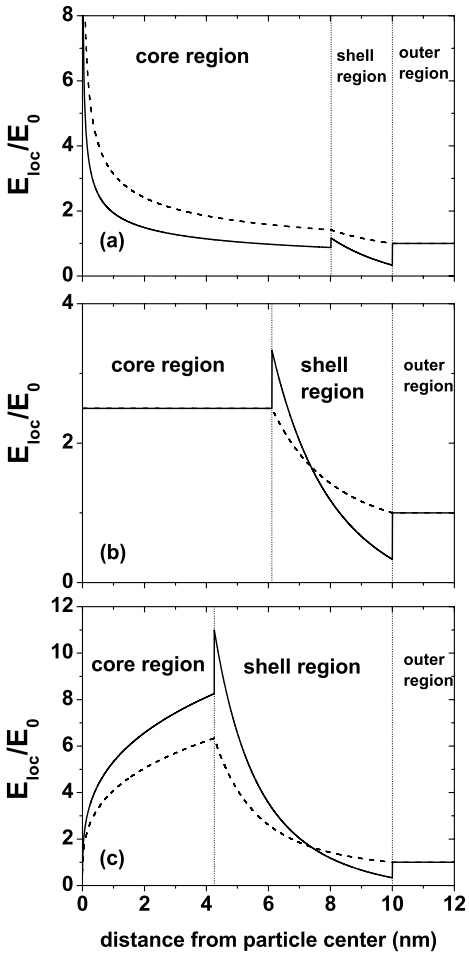

Figure 10 Spatial variation of the electric fields in the presence of a coated particle at the transparency condition for (a) $\epsilon_{\mathrm{ct}} = 2$, (b) $\epsilon_{\mathrm{ct}} = 4$, and (c) $\epsilon_{\mathrm{ct}} = 6$ (reprinted with permission from [87]). The solid curve is for the field parallel to the incident $\boldsymbol{E}_0$, and the dotted line for the one perpendicular to $\boldsymbol{E}_0$. The coated system is nonmagnetic, with parameters $b = 0.1\lambda$, $\lambda = 100$ nm, $\epsilon_{\mathrm{cr}} = 4$, and $\epsilon_{\mathrm{sr}} = \epsilon_{\mathrm{st}} = -3$. The first and second vertical dash-dotted lines respectively correspond to the radii of the core and the shell, in which the ratio is determined by Eq. (52).

5. Enhanced optical nonlinearity in coated RA particles

5.1. Introduction to effective nonlinear susceptibilities

In the static or quasi-static limit, it is known that composite materials may possess strong nonlinear optical properties, e.g., second harmonic generation (SHG) susceptibility and third harmonic generation (THG) susceptibility [89]. The higher-order nth power is also very sensitive to the local field [90].

When we apply a monochromatic external field along the z axis to the composite system, the local potentials and fields will be generated at all harmonic frequencies due to the quadratic nonlinearity of the components inside the composite at finite frequencies [91]. The effective nonlinear SHG susceptibility $d_{\mathrm{e},ijk}^{(\omega,\omega)}$ [92] can be written as

$$d_{\mathrm{e},ijk}^{(\omega,\omega)} = \sum_{\alpha=\mathrm{c}}^{\mathrm{s}} f_\alpha \left\langle K_{il}^{2\omega} (d_{lmn}^{\alpha})^{(\omega,\omega)} K_{jm}^{\omega} K_{kl}^{\omega} \right\rangle_\alpha , \tag{54}$$

© 2010 by WILEY-VCH Verlag GmbH & Co. KGaA, Weinheim

where $\langle \cdots \rangle$ represents the spatial average and f_α stands for the volume fraction of the component α. The local-field factor for the lth Cartesian component of the linear field in the particle is denoted by $K_{il}^{\omega} \equiv E_l(\omega)/E_{0,i}(\omega)$ when the external field E_0 is applied along the the ith direction at frequency ω.

The effective THG susceptibility $\chi_{\mathrm{e},ijkl}^{(\omega,\omega,\omega)}$ can be rewritten as [91]

$$\chi_{\mathrm{e},ijkl}^{(\omega,\omega,\omega)} = \sum_{\alpha=\mathrm{c}}^{\mathrm{s}} f_\alpha \times \left\langle 2K_{im}^{3\omega}(d_{mnp}^{\alpha})^{(\omega,2\omega)} \frac{K_{rn}^{2\omega} - I_{rn}}{\delta(\epsilon^{\alpha})^{(2\omega)}} (d_{rst}^{\alpha})^{(\omega,\omega)} K_{js}^{\omega} K_{kt}^{\omega} K_{lp}^{\omega} \right\rangle_{\alpha}, \quad (55)$$

in which one can observe that the effective third-order nonlinear susceptibility can be induced by the second-order nonlinear response.

5.2. SHG and THG for coated RA particles

The enhanced nonlinear effects using photonic crystals have been reviewed in [93]. For instance, enhanced optical third-order nonlinearity in core-shell structures was discuused in [94], and nonlinear susceptibilities for SHG and THG through core-shell nanostructures were discussed in [95, 96]. However, those constituents are basically isotropic. Anisotropy in the components can also modify optical nonlinearity in the coated RA sphere similarly to Fig. 10. The role of radial anisotropy of individual core-shell constituents will be considered and characterized below. For a dilute suspension of coated RA spheres, the enhanced nonlinear effects have been presented in [32].

In Fig. 11, even though the nonlinearity in the core is weak, the nonlinear effect in the presence of the RA shell is pronounced compared with an 'equivalent' isotropic shell, whose isotropic permittivity $\epsilon_{\mathrm{iso}} = \epsilon_r/3 + 2\epsilon_t/3$ based on the averaging process given in [25].

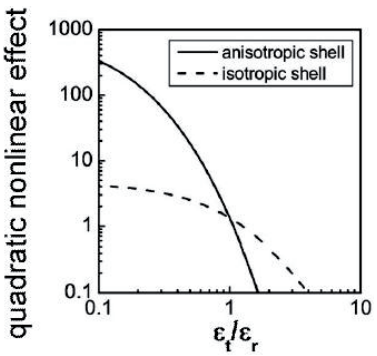

Figure 11 Anisotropy ratio A_{e} dependence of the quadratic nonlinear response per unit volume (reprinted with permission from [32]). The core-shell ratio is 1/4, i.e., the volume fraction of the core-shell system is $\lambda = 1/64$. A linear RA shell (within the region $r_0 < r < R$ and $\epsilon_r = 10$) is coated on a nonlinear core (linear dielectric constant $\epsilon_{\mathrm{c}} = 1$ with susceptibility χ_{c}) in a host medium with $\epsilon_h = 5$.

We continue to study the enhancement of nonlinear effects of similar configurations of coated RA particles in Fig. 11, while we consider dense concentration and induced THG. In addition to ϵ_{c}, the nonlinear core has a second-order susceptibility tensor $\overleftrightarrow{d}_{\mathrm{c}}$, and the RA shell is assumed to be nonmagnetic and linear characterized by Eq. (19) and $\mu_r = \mu_t = 1$. Note that the spherical particles may possess the quadratic nonlinearity due to the fact that the inversion symmetry is broken at the surface [97, 98].

When a monochromatic external field is applied, say along the z axis, we want to solve the potential function in the core, the shell, and the host. Since the coated inclusions are not dilute, the electrostatic dipolar interaction among inclusions should be taken into account. Then, the local fields are affected by the Lorentz field $\boldsymbol{E}_{\mathrm{L1}}$ instead of $\boldsymbol{E}_0$. The solution is as follows:

$$\begin{cases} \phi_{\mathrm{c}} = -A_1 E_{\mathrm{L1}} r\cos\theta\,, & r < r_0\,, \\ \phi_{\mathrm{s}} = -E_{\mathrm{L1}}(B_1 r^{\nu_1} - \dfrac{C_1}{r^{\nu_1+1}})\cos\theta\,, & r_0 < r < R\,, \\ \phi_{\mathrm{m}} = -E_{\mathrm{L1}}(r - \dfrac{P_1 R^3}{Q_1 r^2})\cos\theta\,, & r > R\,, \end{cases} \quad (56)$$

where

$$A_1 = \frac{3\epsilon_h\epsilon_r(2\nu_1+1)\lambda^{(\nu_1-1)/3}}{Q_1}\,,$$

$$B_1 = \frac{3\epsilon_h[\epsilon_r(1+\nu_1)+\epsilon_{\mathrm{c}}]R^{1-\nu_1}}{Q_1}\,,$$

$$C_1 = \frac{-3\epsilon_h\lambda^{(2\nu_1+1)/3}(\epsilon_r\nu_1-\epsilon_{\mathrm{c}})R^{\nu_1+2}}{Q_1}\,,$$

with $\lambda = (r_0/R)^3$ and

$$\nu_1 = \frac{1}{2}\left(\sqrt{1+8\epsilon_t/\epsilon_r}-1\right)\,,$$

$$P_1 = (\epsilon_r\nu_1-\epsilon_h)\left[\epsilon_{\mathrm{c}}+(1+\nu_1)\epsilon_r\right] \lambda^{(2\nu_1+1)/3}\left[\epsilon_h+(1+\nu_1)\epsilon_r\right](\epsilon_{\mathrm{c}}-\epsilon_r\nu_1)\,,$$

$$Q_1 = \left[\epsilon_r(1+\nu_1)+\epsilon_{\mathrm{c}}\right](\epsilon_r\nu_1+2\epsilon_h) \lambda^{(2\nu_1+1)/3}[2\epsilon_h-\epsilon_r(1+\nu_1)](\epsilon_r\nu_1-\epsilon_{\mathrm{c}})\,.$$

The averaged field over the entire system must be equal to $\boldsymbol{E}_0$, so we have

$$f\langle \mathbf{E}_{\mathrm{c1}}\rangle + \left(\frac{f}{\lambda}-f\right)\langle \mathbf{E}_{\mathrm{s1}}\rangle + \left(1-\frac{f}{\lambda}\right)\mathbf{E}_{\mathrm{L1}} = \mathbf{E}_0\,, \quad (57)$$

where f is the volume fraction of the core and

$$\mathbf{E}_{\mathrm{L1}} = \frac{Q_1}{Q_1 - \frac{f}{\lambda}P_1}\mathbf{E}_0\,. \quad (58)$$

© 2010 by WILEY-VCH Verlag GmbH & Co. KGaA, Weinheim

Assuming K_{il}^{ω} to be nonzero only when $i = l$, only d_{zzz}^{e} (SHG) and χ_{zzzz}^{e} (THG) do not vanish in Eqs. (54) and (55), which can be expressed as

$$\frac{d_{zzz}^{\mathrm{e}}}{f d_{zzz}^{(\omega,2\omega)}} = \left\langle K_{1zz}^{2\omega}(K_{1zz}^{\omega})^2 \right\rangle_{\mathrm{c}} = \left(\frac{A_1 Q_1}{Q_1 - \frac{f}{\lambda}P_1}\right)_{2\omega} \left(\frac{A_1 Q_1}{Q_1 - \frac{f}{\lambda}P_1}\right)_{\omega}^{2}, \tag{59}$$

$$\frac{\chi_{zzzz}^{\mathrm{e}}}{f d_{zzz}^{(\omega,2\omega)} d_{zzz}^{(\omega,\omega)}} = \frac{2f\langle K_{1zz}^{3\omega}(K_{1zz}^{2\omega}-1)(K_{1zz}^{\omega})^3\rangle_{\mathrm{c}}}{\epsilon_{\mathrm{c}}^{2\omega} - \epsilon_{\mathrm{e1}}^{2\omega}} = \frac{2f}{\epsilon_{\mathrm{c}}^{2\omega} - \epsilon_{\mathrm{e1}}^{2\omega}} \left(\frac{A_1 Q_1}{Q_1 - \frac{f}{\lambda}P_1}\right)_{3\omega} \times \left(\frac{A_1 Q_1}{Q_1 - \frac{f}{\lambda}P_1}\right)_{\omega}^{3} \times \left[\left(\frac{A_1 Q_1}{Q_1 - \frac{f}{\lambda}P_1}\right)_{2\omega} - 1\right], \tag{60}$$

where

$$\epsilon_{\mathrm{e1}}^{2\omega} = \left[\epsilon_{\mathrm{m}} + 3\frac{f}{\lambda}\epsilon_{\mathrm{m}}\frac{P_1}{Q_1 - \frac{f}{\lambda}P_1}\right]_{2\omega}. \tag{61}$$

In our model, the core is a Drude metal:

$$\epsilon_{\mathrm{c}}(\omega) = 1 - \frac{\omega_{\mathrm{p}}^2}{\omega^2 + i\omega/\tau},$$

with ω_{p} being the plasma frequency and τ the relaxation time. We take $\omega_{\mathrm{p}} = 2.28\times10^{16}\,\mathrm{s}^{-1}$ and $\tau = 6.9\times10^{-15}\,\mathrm{s}$, corresponding to bulk aluminum. The anisotropic shell is assumed to have a frequency-independent radial dielectric constant $\epsilon_r = 2.52$, while the host medium also has a frequency-independent dielectric constant $\epsilon_h = 1.76$. These numbers are typical for nonconducting materials.

In Fig. 12, it is evident that there are two peaks in d_{zzz}^{e}. The bigger one may be of the order 10^3–10^4 and is located at the surface plasmon frequency ω_{sp} while the other is located at about $\omega_{\mathrm{sp}}/2$. This is due to the fact that the SHG susceptibility intrinsically involves two different frequencies. It is interesting to note that when the anisotropy ratio decreases, the surface plasmon resonances ω_{sp} exhibit blue shifts, accompanied with large enhancement of the SHG susceptibility. It can also be found that the nonlinearity enhancement in the nondilute limit is larger than the one in the dilute limit [32, 95].

Although the material has second-order nonlinearity only, the composite may exhibit third-order nonlinearity. The induced third-order nonlinear susceptibility is presented in Fig. 13. An enhancement factor of the order of 10^5 is achieved at suitable frequencies. In this situation, there

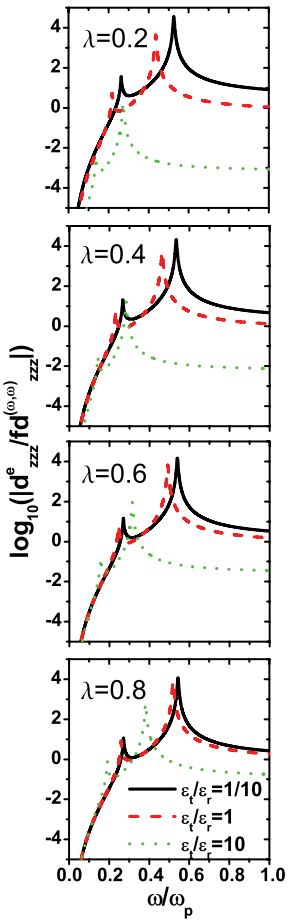

Figure 12 (online color at: www.lpr-journal.org) The enhancement of effective SHG susceptibility $|d_{zzz}^{\mathrm{e}}/f d_{zzz}|$ versus the normalized incident angular frequency $\omega/\omega_{\mathrm{p}}$ for various interfacial parameters λ at three anisotropic ratios when the volume fraction of the coated particles is 0.1.

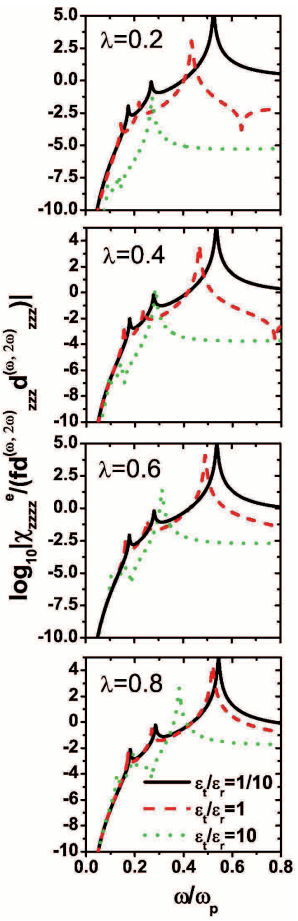

Figure 13 (online color at: www.lpr-journal.org) The enhancement of the induced third-order nonlinear susceptibility $\chi_{zzzz}^{\mathrm{e}}/f d_{zzz}^{(\omega,2\omega)} d_{zzz}^{(\omega,\omega)}$, the other settings being the same as Fig. 12.

are three enhancement peaks in χ_{zzzz}^{e}, and the dominant one is located at the shifted resonant frequency ω_{sp}. The reason is that the nonlinear optical process leads to a 3ω component by combining a 2ω component, which is formed first, with a ω component. The larger effective THG susceptibility is found at the high frequencies when $A_{\mathrm{e}} = \epsilon_t/\epsilon_r$ is small. Again, we demonstrate that the anisotropy plays an important role in the enhancement of optical nonlinearities at the surface resonant frequencies.

6. Discussion and conclusion

In this review, we started from the preliminaries in anomalous light scattering from isotropic 3D particles, and then

© 2010 by WILEY-VCH Verlag GmbH & Co. KGaA, Weinheim

introduced the anisotropy into the material. Two different types of anisotropy have been considered in Cartesian and spherical coordinates, respectively. The role of anisotropy in scattering properties is characterized both analytically and numerically. Radial anisotropy (RA) has opened a new window of opportunity not only in the area of plasmonic scattering but also in the field of nonlinear photonics. In the core-shell system, the RA shell provides a totally independent way to control the wave propagation path in and around the particle, the scattering efficiencies in the far zone, and effective nonlinear susceptibilities for SHG and induced THG. The adjustment of RA may result in nondissipative damping, invisibility, and/or large enhancement of both SHG and induced THG susceptibilities at surface plasmon resonant frequencies. Thus, the theoretical modeling for RA particles or photonic crystals with RA is likely to have a significant impact in providing guidelines for future technology and fabrication for cloaking devices and nonlinear optics.

Another issue of practical importance is where to find those candidates with RA in nature and/or how to design and fabricate them artificially. As mentioned, such RA can be found in biological tissues such as a human brain [9], orientational molecules [10], and phospholipid vesicles [99]. Material scientists also discovered that the onion-like multiple graphite shells exhibit dielectric anisotropy [100]. Recently, experiments revealed that such RA can be realized by an anisotropic nematic liquid crystal coated on a nanoparticle [101, 102], where the surface plasmon resonances were also found to be split as discussed in this review. However, the dielectric response for nematic liquid crystals is complex in general, which depends on temperature, direction of the static field, etc. Then, the thin layer of ordered molecules such as chromophores [103], whose the local optical axis is pointing along the radial direction, appears to be an alternative good candidate of the desired RA. We hope that our summary will be helpful to facilitate the exploration in this exciting area of dielectric anisotropy as well as to improve the experimental investigation of magnetic anisotropy.

Chengwei Qiu was born in Zhejiang, China on March 9, 1981. He received the B.Eng. degree from the University of Science and Technology of China in 2003, and the Ph. D. degree from the Joint Ph. D. Program between the National University of Singapore, Singapore and SUPELEC, France in 2007. His research interests are in the areas of electromagnetic wave theory of complex media (e.g., chiral, anisotropic, and bianisotropic materials), invisibility cloaks, and metamaterials. He has published over 30 journal papers and one book chapter, and has given invited talks at conferences. He was the recipient of the SUMMA Graduate Fellowship in Advanced Electromagnetics in 2005. He was also the recipient of the IEEE AP-S Graduate Research Award in 2006. In 2007, he received a Young Scientist Travel Grant for ISAP2007 in Niigata, Japan, and a Travel Grant for Metamaterial'07 in Rome, Italy. In 2008, he received a URSI Young Scientist Award in Chicago. From 2009, he has been a postdoctoral fellow in the Research Laboratory of Electronics at Massachusetts Institute of Technology (MIT).

John D. Joannopoulos was born in New York, NY, on April 26, 1947. He received his B. A. and Ph. D. degrees in physics from the University of California, Berkeley in 1968 and 1974, respectively. He has been on the Faculty of Physics at the Massachusetts Institute of Technology as Assistant Professor of Physics (1974), Associate Professor of Physics (1978), and Professor of Physics (1983), and was awarded the Francis Wright Davis Professor of Physics Chair in 1996. He has served as Divisional Associate Editor of Physical Review Letters, a member of the Editorial Board of Reviews of Modern Physics, and was appointed as the Director of the Institute for Soldier Nanotechnologies in 2006. His research spans a variety of topics in theoretical condensed matter physics including electronic, vibrational, magnetic, and photonic structure in solids. He is the author or coauthor of over 500 refereed scientific journal articles, three textbooks on photonic crystals, and holds over 50 issued U. S. patents. He is also co-founder of three startup companies: OmniGuide, Inc., Luminus Devices, Inc., and WiTricity Corporation.

Lei Gao was born in Jiangsu Province, the People's Republic of China on February 15, 1971. He received the B. S., the M. S., and the Ph. D. degrees from Soochow University in 1992, 1997, and 2000, respectively. During 1992–1994, he served as a teacher of physics in Xinyi Middle School. After 2000, he joined the Department of Physics, Soochow University as a Research Assistant. Since 2002, he has been a Professor in Soochow University, where his research activities concentrate on condensed matter theory and nonlinear optics.

© 2010 by WILEY-VCH Verlag GmbH & Co. KGaA, Weinheim

Marin Soljacic has been an Assistant Professor of Physics since September 2005. He received a BsE degree in physics and electrical engineering from MIT in 1996, and earned his Ph. D. degree in physics at Princeton University in 2000. In September 2000, he was named an MIT Pappalardo Fellow in Physics, and in 2003 was appointed a Principal Research Scientist in the Research Laboratory of Electronics at MIT. His main research interests are in theory of electromagnetic phenomena, focusing on nanophotonics, non-linear optics, and wireless power transfer. He is a co-author of 88 scientific articles and 15 patents, and has given more than 40 invited talks at conferences and universities around the world. He is the recipient of the Adolph Lomb medal from the Optical Society of America (2005), and the TR35 award of the Technology Review magazine (2006). The work on wireless power transfer that he pioneered has been singled out as one of the most important technological developments of 2007 by the New York Times, BBC News, Scientific American, Technology Review, and Discover magazine. In 2008, he was given a MacArthur fellowship award.

References

[1] L. Lorentz, Vidensk. Selk. Skr. **6**, 1 (1890).
[2] G. Mie, Ann. Phys. (Leipzig) **25**, 377 (1908).
[3] B. S. Luk'yanchuk and V. Ternovsky, Phys. Rev. B **73**, 235432 (2006).
[4] B. S. Luk'yanchuk, M. I. Tribelsky, Z. B. Wang, Y. Zhou, M. H. Hong, L. P. Shi, and T. C. Chong, Appl. Phys. A **89**, 259 (2007).
[5] M. I. Tribelski, S. Flach, A. E. Miroshnichenko, A. V. Gorbach, and Y. S. Kivshar, Phys. Rev. Lett. **100**, 043903 (2008).
[6] W. Fang, J. Y. Xu, A. Yamilov, H. Cao, Y. Ma, S. T. Ho, and G. S. Solomon, Opt. Lett. **27**, 948 (2002).
[7] M. Gottlied, C. L. M. Ireland, and J. M. Ley, Electro-Optic and Acousto-Optic Scanning and Deflection, Optical Engineering Series (Marcel Dekker, New York, 1983).
[8] A. A. Lukas, L. Henrard, and Ph. Lambin, Phys. Rev. B **49**, 2888 (1993).
[9] J. C. E. Sten, IEEE Trans. Dielectr. Electr. Insul. **2**, 360 (1995).
[10] V. L. Sukhorukov, G. Meedt, M. Kurschner, and U. Zimmermann, J. Electrostat. **50**, 191 (2001).
[11] Y. L. Geng, X. B. Wu, L. W. Li, and B. R. Guan, Phys. Rev. E **70**, 056609 (2004).
[12] A. McWilliams and M. Rauch (eds.), Origin and Evolution of the Elements (Cambridge University Press, Cambridge, New York, 2004), p. 230.
[13] B. Stout, M. Nevière, and E. Popov, J. Opt. Soc. Am. A **23**, 1111 (2006).
[14] B. Stout, M. Nevière, and E. Popov, J. Opt. Soc. Am. A **23**, 1124 (2006).
[15] J. Roth and M. J. Dignam, J. Opt. Soc. Am. **63**, 308 (1973).
[16] J. C. Monzon, IEEE Trans. Antennas Propag. **37**, 728 (1989).
[17] A. D. Kiselev, V. Yu. Reshetnyak, and T. J. Sluckin, Phys. Rev. E **65**, 056609 (2002).
[18] M. F. Yanik, H. Cinar, N. Cinar, A. Chisholm, Y. Jin, and A. Ben-Yakar, Nature **432**, 822 (2004).
[19] R. D. Weglein, Appl. Phys. Lett. **34**, 179 (1979).
[20] J. Kushibiki, A. Ohkubo, and N. Chubachi, Electron. Lett. **17**, 534 (1981).
[21] A. C. Guo, J. R. Petrella, J. Kurtzberg, and J. M. Provenzale, Radiology **218**, 809 (2001).
[22] S. Hashimoto, Y. Ochiai, and K. Aso, J. Appl. Phys. **66**, 4909 (1989).
[23] A. B. MacIsaac, K. De'Bell, and J. P. Whitehead, Phys. Rev. Lett. **80**, 616 (1998).
[24] T. Eimuller, T. C. Ulbrich, E. Amaladass, I. L. Guhr, T. Tyliszczak, M. Albrecht, Phys. Rev. B **77**, 134415 (2008).
[25] C. F. Bohren and D. R. Huffman, Absorption and Scattering of Light by Small Particles (Wiley, New York, 1998).
[26] J. B. Pendry, D. Schurig, and D. R. Smith, Science **312**, 1780 (2006).
[27] A. Hendi, J. Henn, and U. Leonhardt, Phys. Rev. Lett. **97**, 073902 (2006).
[28] R. Weder, J. Phys. A, Math. Theor. **41**, 065207 (2008).
[29] J. Hu, X. Zhou, and G. Hu, Opt. Express **17**, 1308 (2009).
[30] C. W. Qiu, L. Hu, X. Xu, and Y. Feng, Phys. Rev. E, to appear (2009).
[31] B. Luk'yanchuk and C. W. Qiu, Appl. Phys. A **92**, 773 (2008).
[32] D. H. Liu, C. Xu, and P. M. Hui, Appl. Phys. Lett. **92**, 181901 (2008).
[33] D. J. Wu and X. J. Liu, Appl. Phys. A **94**, 537 (2009).
[34] W. Zhang and D. H. Liu, Solid State Commun. **149**, 146 (2009).
[35] M. Born and E. Wolf, Principles of Optics, 7th edn. (Cambridge University Press, Cambridge, New York, 1999).
[36] H. J. Münzer, M. Mosbacher, M. Bertsch, J. Zimmermann, P. Leiderer, and J. Boneberg, J. Microsc. **202**, 129 (2001).
[37] H. J. Munzer, J. Zimmermann, J. Solis, J. Boneberg, and P. Leiderer, Appl. Phys. A **72**, 41 (2001).
[38] K. Piglmayer, R. Denk, and D. Bäuerle, Appl. Phys. Lett. **80**, 4693 (2002).
[39] F. Lang, M. Mosbacher, and P. Leiderer, Appl. Phys. A **77**, 117 (2003).
[40] M. G. Capeluto, P. W. Wachulak, M. C. Marconi, D. Patel, C. S. Menoni, J. J. Rocca, C. Iemmi, E. H. Anderson, W. Chao, and D. T. Attwood, Microelectron. Eng. **84**, 721 (2007).
[41] Yu. A. Kravtsov and Yu. I. Orlov, Geometrical Optics of Inhomogeneous Media (Springer, Berlin, 1990).
[42] N. Arnold, Appl. Surf. Sci. **208–209**, 15 (2003).
[43] N. P. Kerk, J. N. L. Connor, P. R. Curtis, and C. A. Hobbs, J. Phys. A, Math. Gen. **33**, 4797 (2000).
[44] R. E. Hamam, A. Karalis, J. D. Joannopoulos, and M. Soljačić, Phys. Rev. A **75**, 053801 (2007).
[45] M. I. Tribelski and B. S. Luk'yanchuk, Phys. Rev. Lett. **97**, 263902 (2006).
[46] U. Fano, Phys. Rev. **124**, 1866 (1961).

© 2010 by WILEY-VCH Verlag GmbH & Co. KGaA, Weinheim

[47] G. C. Seckin and Y. Erdem, IEEE Trans. Antennas Propag. **52**, 2532 (2004).
[48] B. I. Wu, W. Wang, J. Pacheco, X. Chen, J. Lu, T. M. Grzegorczyk, J. A. Kong, P. Kao, P. A. Theophelakes, and M. J. Hogan, Microwave Opt. Tech. Lett. **48**, 680 (2006).
[49] M. L. Tounsi, R. Touhami, A. Khodja, and M. C. E. Yagoub, Prog. Electromagn. Res. **62**, 281 (2006).
[50] C. Wang, Y. Zhao, D. Gan, C. Du, and X. Luo, Opt. Express **16**, 4217 (2008).
[51] H. Liu, Shivanand, and K. J. Webb, Opt. Lett. **33**, 2568 (2008).
[52] L. Hu and Z. Lin, Phys. Lett. A **313**, 316 (2003).
[53] C. W. Qiu, H. Y. Yao, L. W. Li, S. Zouhdi, and T. S. Yeo, Phys. Rev. B **75**, 155120 (2007).
[54] C. W. Qiu, H. Y. Yao, L. W. Li, S. Zouhdi, and T. S. Yeo, Phys. Rev. B **75**, 245214 (2007).
[55] X. Xu, Y. Feng, and T. Jiang, arXiv:0806.0893 (2008).
[56] H. Chen and C. T. Chan, Appl. Phys. Lett. **91**, 183518 (2007).
[57] W. Ren, Phys. Rev. E **47**, 664 (1993).
[58] A. L. Efros and A. V. Rodina, Phys. Rev. B **47**, 10005 (1993).
[59] J. L. Volakis, G. Mumcu, K. Sertel, C. C. Chen, M. Lee, B. Kramer, D. Psychoudakis, and G. Kizitaz, IEEE Antennas Propag. Mag. **48**, 12 (2006).
[60] A. A. Chabanov, in: Photonic Metamaterials: From Random to Periodic, Jackson Hole, WY, OSA Tech. Digest, paper TuB10 (2007).
[61] R. E. Colin, IEEE Trans. Microw. Theory Tech. **6**, 206 (1958).
[62] R. D. Graglia, P. L. E. Uslenghi, and R. S. Zich, Proc. IEEE **77**, 750 (1989).
[63] H. X. Zhang, X. Q. Sheng, and E. K. N. Yung, Prog. Electromagn. Res. **35**, 287 (2002).
[64] A. F. Yagli, Ph. D. thesis, Syracuse University, Syracuse, NY (2006).
[65] B. Beker, Ph. D. thesis, University of Illinois at Chicago, Chicago, IL (1988).
[66] V. V. Varadan, A. Lakhtakia, and V. K. Varadran, IEEE Trans. Antennas Propag. **37**, 800 (1989).
[67] S. N. Papadakis, N. K. Uzunoglu, and C. N. Capsalis, J. Opt. Soc. Am. A **7**, 991 (1990).
[68] W. C. Chow, Waves and Fields in Inhomogeneous Media (Van Nostrand, New York, 1990).
[69] C. T. Tai, Dyadic Green's Functions in Electromagnetic Theory (IEEE Press, New York, 1993).
[70] D. H. Schaubert, D. R. Wilton, and A. W. Glisson, IEEE Trans. Antennas Propag. **32**, 276 (1984).
[71] D. H. Schaubert, D. R. Wilton, and A. W. Glisson, IEEE Trans. Antennas Propag. **32**, 77 (1984).
[72] A. Lakhtakia, Int. J. Mod. Phys. C **3**, 583 (1992).
[73] C. C. Su, IEEE Trans. Antennas Propag. **37**, 384 (1989).
[74] X. Q. Zhu, Y. L. Geng, and X. B. Wu, Chin. J. Radio Sci. **17**, 209 (2002).
[75] G. Kobidze and B. Shanker, IEEE Trans. Antennas Propag. **52**, 2650 (2004).
[76] B. C. Usner, K. Sertel, and J. L. Volakis, IET Microw. Antennas Propag. **1**, 150 (2007).
[77] W. A. de Heer and D. Ugarte, Chem. Phys. Lett. **207**, 480 (1993).
[78] J. Helsing and A. Helte, J. Appl. Phys. **69**, 3583 (1991).
[79] J. C. de Munck, J. Appl. Phys. **64**, 464 (1988).
[80] C. W. Qiu, L. W. Li, Q. Wu, and T. S. Yeo, IEEE Antennas Wireless Propag. Lett. **4**, 467 (2005).
[81] C. W. Qiu, L. W. Li, T. S. Yeo, and S. Zouhdi, Phys. Rev. E **75**, 026609 (2007).
[82] L. D. Landau, Sov. Phys. JETP **16**, 574 (1946).
[83] K. Busch and S. John, Phys. Rev. Lett. **83**, 967 (1999).
[84] A. Moroz, Phys. Rev. B **66**, 115109 (2002).
[85] S. Liu and Z. Lin, Phys. Rev. E **73**, 066609 (2006).
[86] H. S. Chen, B. I. Wu, B. L. Zhang, and J. A. Kong, Phys. Rev. Lett. **99**, 0663903 (2007).
[87] L. Gao, T. H. Fung, K. W. Yu, and C. W. Qiu, Phys. Rev. E **78**, 046609 (2008).
[88] Y. Wu, J. Li, Z. Q. Zhang, and C. T. Chan, Phys. Rev. B **74**, 085111 (2006).
[89] O. Levy, D. J. Bergman, and D. Stroud, Phys. Rev. E **52**, 3184 (1995).
[90] V. M. Shalaev, E. Y. Poliakov, and V. A. Markel, Phys. Rev. B **53**, 2437 (1996).
[91] P. M. Hui, P. Cheng, and D. Stroud, J. Appl. Phys. **84**, 3451 (1998).
[92] P. M. Hui and D. Stroud, J. Appl. Phys. **82**, 4740 (1997).
[93] M. Soljacic and J. D. Joannopoulos, Nature Mater. **3**, 211 (2004).
[94] A. E. Neeves and M. H. Birnboim, J. Opt. Soc. Am. B **6**, 787 (1989).
[95] P. M. Hui, C. Xu, and D. Stroud, Phys. Rev. B **69**, 014203 (2004).
[96] Y. Yang, M. Hori, T. Hayakawa, and M. Nogami, Surf. Sci. **579**, 215 (2005).
[97] J. I. Dadap, J. Shan, K. B. Eisenthal, and T. F. Heinz, Phys. Rev. Lett. **83**, 4045 (1999).
[98] N. Yang, W. E. Angerer, and A. G. Yodh, Phys. Rev. Lett. **87**, 103902 (2001).
[99] B. Lange and S. R. Aragon, J. Chem. Phys. **92**, 4643 (1990).
[100] D. Ugarte, Nature **359**, 707 (1992).
[101] J. Müller, C. Sönnichsen, H. V. Poschinger, G. V. Plessen, T. A. Klar, and J. Feldmann, Appl. Phys. Lett. **81**, 171 (2002).
[102] S. Y. Park and D. Stroud, Phys. Rev. Lett. **94**, 217401 (2005).
[103] T. Ambjörnsson, G. Mukhopadhyay, S. P. Apell, and M. Käll, Phys. Rev. B **73**, 085412 (2006).

© 2010 by WILEY-VCH Verlag GmbH & Co. KGaA, Weinheim